Viggo Tvergaard
Department of Mechanical Engineering,
Technical University of Denmark,
Lyngby 2800, Denmark

John W. Hutchinson
School of Engineering and Applied Sciences,
Harvard University,
Cambridge, MA 02138-2933

Numerical Simulation of Cropping

Cropping is a cutting process whereby opposing aligned blades create a shearing failure by exerting opposing forces normal to the surfaces of a metal sheet or plate. Building on recent efforts to quantify cropping, this paper formulates a plane strain elastic–plastic model of a plate subject to shearing action by opposing rigid platens. Shear failure at the local level is modeled by a cohesive zone characterized by the peak shear traction and the energy dissipated by shear failure process at the microscopic level. The model reveals the interplay between shear cracking and the extensive plastic shearing accompanying the cutting process. Specifically, it provides insight into the influence of the material's microscopic shear strength and toughness on the total work of cropping. The computational model does not account for deformation of the cropping tool, friction between sliding surfaces, and material temperature and rate dependence. [DOI: 10.1115/1.4026891]

Keywords: cropping, shear fracture, finite strain plasticity, cohesive zone, fracture energy

1 Background to the Present Study

Cutting by forced shear-off, often called blanking or cropping, is widely employed to cut flat sheets and plates of structural metals having thickness ranging from submillimeter to 10 mm or more. Forced shear-off can also occur in the plugging process in ballistic penetration when a high velocity projectile impacts a plate. The simplest notions of cropping imagine that the process is essentially a shear failure within a localized shear band that is primarily controlled by the shear strength of the material. The present paper continues the line of investigation initiated in a series of papers by Atkins [1–4] who takes the view that shear cracking and material shear toughness play an essential role in the cropping process and in determining the energy required for cropping. The series of Atkins' papers presents models of cropping with an increasing level of sophistication without recourse to finite element models of finite plastic straining. An early paper by Zhou and Wierzbicki [5] also employs analytical modeling and accounts for tensile fracture as well as shearing in the cropping process, which in their paper and in some of the earlier literature is referred to as blanking.

Following Atkins, the view adopted in this paper is that cropping is a large scale yielding fracture problem dominated by shear. As in the case of the present authors' earlier work on elastic–plastic crack growth in mode I [6] and mixed mode [7], the present paper exploits the finite element analysis to deal with large plastic strains. The present paper also makes use of recent developments in modeling fracture under shear dominated conditions. The cropping model developed here imbeds a cohesive shearing zone, which, in a phenomenological manner, represents the microscopic shear localization and fracture processes, within a finite element model that accounts for the geometric distribution of the large plastic shear strains that occur in the cropping process. The model quantifies the interplay between the microscopic shearing failure process and the extensive macroscopic plastic shearing. A systematic study is made of the effects of the microscopic fracture energy and the material stress–strain properties on the cropping force– displacement behavior and the macroscopic cropping energy.

Alternative approaches to studying cropping could be based on analyses that adopt either a critical effective plastic strain as a failure criterion or a constitutive law that incorporates damage and a failure criterion. When carefully calibrated, the critical plastic strain criterion has proved effective in the studies of ballistic plugging of plates by projectiles, e.g., Borvik et al. [8,9] and Nahshon et al. [10]. Xue et al. [11] demonstrated the applicability to ballistic shear-off of the Gurson model [12,13] of void-based damage and failure, extended to account for damage in shear. A distinct advantage of the cohesive zone model adopted in the present paper is that the microscopic strength and fracture energy are well defined parameters and their role in establishing macroscopic behavior clearly emerges.

1.1 An Illustrative Cropping Experiment. Xue et al. [11] carried out carefully designed cropping tests on plates of the steel DH 36 of thickness $h = 3\,\text{mm}$. As illustrated in Fig. 1, the tests provided the response of a hard tool steel cylindrical plunger pushing against a plate clamped tightly outside the plunger radius by a stiff fixture. The nominal shear stress supported by the plate at radius R, $P/(2\pi Rh)$, is plotted as a function of the plunger displacement divided by the plate thickness Δ/h for one test in Fig. 1(*b*). The peak nominal shear stress is about 420 MPa at $\Delta/h \cong 0.25$. The largest plunger displacement shown is $\Delta/h \cong 0.55$. The load drops precipitously at larger displacements such that the macroscopic work of cropping is directly related to the area under the curve in Fig. 1(*b*). Tests were interrupted at various stages and cross sections of the sheared-off region were opened to viewing by electrodischarge machining (EDM). In addition to intense plastic shearing throughout the region of shear-off, shear cracks are observed. Examples of shear cracks near the corner of the plunger at $\Delta/h = 0.5$ are seen in Fig. 1(*d*), where it is noted that some cracks form slightly offset from the line extending the corner of the plunger.

The radius of the plunger in the Xue et al. [11] test is sufficiently large compared to the plate thickness, i.e., $R/h = 6.3$, such that it is reasonable to assume that the specific cropping work Γ_{CROP}, with units work/area cut, would be nearly the same as that measured for a long straight cut. The total work done by the plunger in Fig. 1(*b*) is $W = \alpha 2\pi R h^2 (\bar{\tau}_Y)_{\text{MAX}}$, where $(\bar{\tau}_Y)_{\text{MAX}}$ is the maximum nominal shear stress and α is a dimensionless numerical factor that depends on the parameters of the system. The specific cropping work (per area cut) is

$$\Gamma_{\text{CROP}} = \frac{W}{2\pi R h} = \alpha (\bar{\tau}_Y)_{\text{MAX}} h \qquad (1)$$

Manuscript received January 9, 2014; final manuscript received February 14, 2014; accepted manuscript posted February 21, 2014; published online March 6, 2014. Editor: Yonggang Huang.

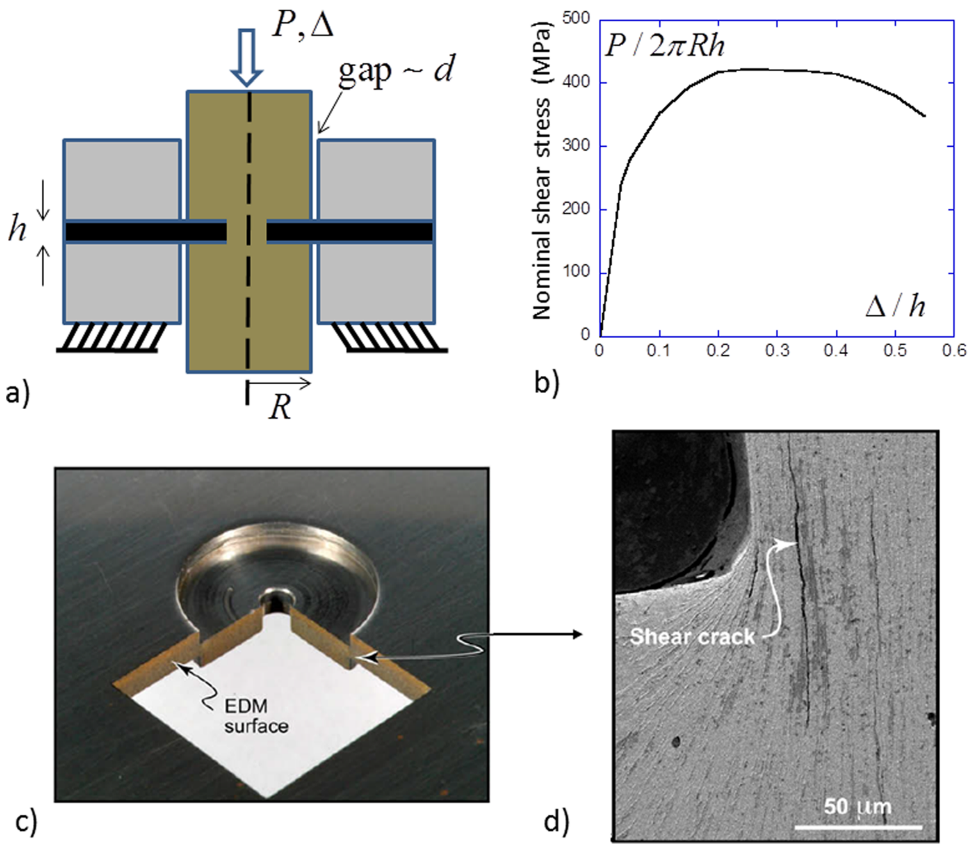

Fig. 1 A cropping shear-off test of Xue et al. [11]. (*a*) Schematic of the axisymmetric test configuration. The two sections of central plunger are bolted together through the center of the plate whose thickness is *h*. (*b*) An experimentally measured nominal shear stress $P/(2\pi Rh)$ versus normalized displacement of the plunger Δ/h for the steel DH 36. For this test: $h = 3$ mm, R=19.05 mm, and the gap width is $d \cong 0.075$ mm. Beyond $\Delta/h = 0.55$, the curve drops precipitously. (*c*) A test interrupted at $\Delta/h = 0.5$ with a section removed from the plate to reveal the details of the shear-off process. (*d*) A blow up of the region at the corner of the plunger showing that shear cracks have formed, some of which are offset from the corner.

For the 3 mm thick plate of DH 36 in Fig. 1(*b*), $(\bar{\tau}_Y)_{\mathrm{MAX}} = 420$ MPa and the area under the load–displacement curve implies $\alpha \cong 1/2$, such that $\Gamma_{\mathrm{CROP}} \cong 6 \times 10^5\ \mathrm{Jm}^{-2}$. This value is consistent with the specific work of cropping reported for other metals in the early work of Johnson and Slater [14] discussed in [4,5].

One of the aims of this paper is to relate the specific macroscopic work of cropping Γ_{CROP} to the specific microscopic work of shear fracture of the material Γ_0, both of which are measured in units of energy/area, Jm^{-2}. Figure 2 presents simulations based on the extended Gurson model [13] for the shear stress–strain behavior accounting for damage in the form of voids with an initial effective volume fraction f_0. A pure power-law material is used to describe the undamaged material in the Gurson model with a tensile relation between the true stress and logarithmic strain given by $\sigma = \sigma_R \varepsilon^N$. The extended model accounts for progressive shear damage, due to shear distortion of the voids, in a phenomenological manner such that in shear (with zero stress triaxiality) damage grows according to $\dot{f} = k_\omega f \dot{\gamma}$, with γ as the logarithmic shear strain and k_ω as the shear damage coefficient [13,15,16]. The trends in Figs. 2(*a*) and 2(*b*) should only be regarded as qualitative since no effort has been made to include the final coalescence stage of the shear failure process. Moreover, microscopic mechanisms other than the void mechanism may be responsible for softening and shear localization. Nevertheless, the results illustrate the roles of damage f_0 and damage growth susceptibility as measured by k_ω in determining the peak shear stress at which point shear localization would begin. This stress–strain behavior has been used to compute the work dissipated in shearing *subsequent to attainment of the peak shear stress* in a shear band of thickness D. Figure 2(*c*) presents the specific work dissipated in the shear band per area Γ_0, normalized by $\sigma_R D$, as a function of the shear damage coefficient for several values of the initial damage. We emphasize that the purpose of Fig. 2 is not to present quantitatively reliable predictions for the shear response or the work dissipated in a shear band but, rather, to suggest trends and to provide rough estimates.

Figure 2(*c*) indicates that the specific work of shear fracture scales as

$$\Gamma_0 = \beta \sigma_R D \tag{2}$$

where β is a factor of order unity depending on the initial damage level and the susceptibility of the damage to shearing as modeled here by the coefficient k_ω. For materials failing by the mechanism of void nucleation, shear distortion, and coalescence, the thickness D of the shear localization zone before the final coalescence stage is usually on the order of the spacing between the dominant voids. Thus, for many ductile alloys, D is typically measured in tens of microns. Assume this is so for DH 36, and note also that for this material the tensile stress at a log strain extrapolated to unity is $\sigma_R \approx 1000$ MPa. With $\beta = 2$ in (2), this implies for DH 36 that Γ_0 is estimated to lie within the range $2 \times 10^4\ \mathrm{Jm}^{-2}$ (for $D = 10\ \mu$m) to $1 \times 10^5\ \mathrm{Jm}^{-2}$ (for $D = 50\ \mu$m). The specific macroscopic work of cropping (1) for the 3 mm plate of DH 36 was estimated to be $\Gamma_{\mathrm{CROP}} \cong 6 \times 10^5\ \mathrm{Jm}^{-2}$. This comparison suggests that the work of cropping is at least 6 times, and possibly as much at 30 times,

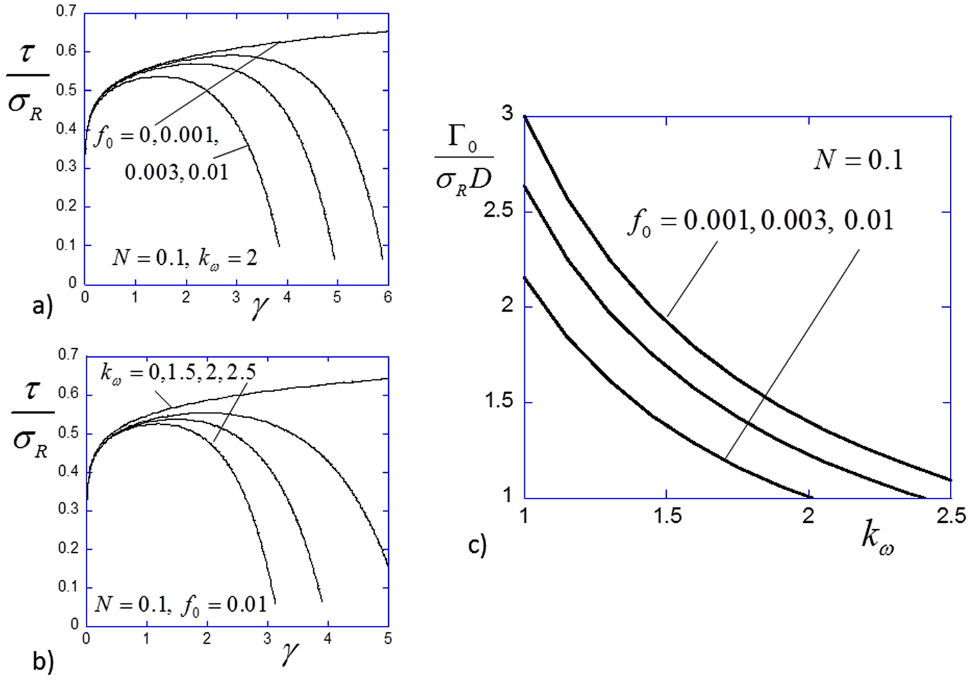

Fig. 2 (*a*) and (*b*) True shear stress versus log shear strain predicted by the extended Gurson model as dependent on the initial effective void volume fraction f_0 and shear damage coefficient k_ω. The reference stress σ_R is defined in the text. (*c*) The normalized specific work of shear separation $\Gamma_0/\sigma_R D$, which is computed for shearing beyond the peak shear stress assuming shearing takes place in a layer of thickness *D*. For this model, the normalized work is only weakly dependent on the strain hardening exponent *N*.

the specific microscopic work of shear fracture for DH 36. If this comparison is correct, it suggests that the major part of the work of cropping is due to plastic deformation occurring outside the shear fracture zone. This relation between the microscopic and macroscopic fracture work is similar to that in mode I crack advance in tough ductile alloys where the macroscopic work of fracture far exceeds the microscopic work of fracture due to plastic dissipation occurring outside the fracture process zone [6]. Nevertheless, in mode I cracking the microscopic work of fracture remains essential in determining the macroscopic toughness, and it will be seen that a similar dependency holds for cropping.

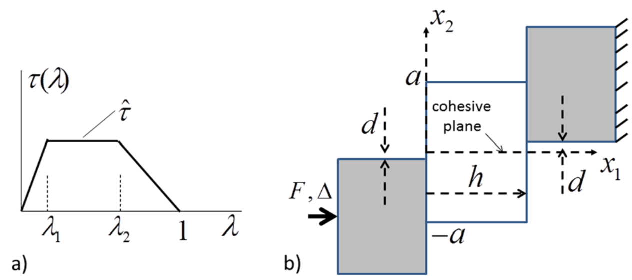

Fig. 3 (*a*) The cohesive traction–displacement relation in shear. (*b*) The undeformed geometry of the numerical model showing the reference coordinates. The cohesive plane in the undeformed state lies along the x_1 axis. The bottom surface along $x_2 = -a$ is constrained to undergo frictionless sliding with zero vertical displacement. The upper surface along $x_2 = a$ is traction-free. Sliding is suppressed at the contact surfaces between the rigid tools and the metal block.

2 Definition of the Model and Dimensionless Parameters

To set the stage for the computational results presented in subsequent sections, the material and geometric parameters governing the cropping model used in this paper will now be listed and the important dimensionless collections of these parameters will be identified. The plate being cut is taken to be isotropic with Young's modulus E, Poisson's ratio ν, initial tensile yield stress σ_Y, initial shear yield stress $\tau_Y = \sigma_Y/\sqrt{3}$, and strain hardening exponent N. In this paper no attempt will be made to account for temperature or rate effects in cropping. The process is modeled as quasi-static and the plate material is taken to be rate independent, excluding any direct relevance to cropping at high temperatures. Elasticity of the cropping tool is also neglected in this study—the surfaces of the cutting tool are taken to be nondeforming. As depicted in Figs. 1(*a*) and 3(*b*), the thickness of the plate is h and the gap between the surfaces of the cropping tool is d. The band of localized shear and shear fracture will be modeled by a cohesive zone whose primary parameters are the peak shear stress $\hat{\tau}$, and the specific work of fracture in shear Γ_0. Full details of the cohesive zone will be given in the next section, including the maximum shearing displacement across the zone prior to loss of shear strength. The maximum shearing displacement can be expressed in terms of $\hat{\tau}$ and Γ_0, which are preferred for specifying the cohesive law in the present study.

It is useful to define the following material reference length:

$$R_S = \frac{1}{\pi(1-\nu^2)}\frac{E\Gamma_0}{\tau_Y^2} \tag{3}$$

which is can be interpreted as the extent of the plastic zone ahead of a mode II (shear) crack in plane strain small scale yielding when subject to the mode II stress intensity factor $K_{II} = \sqrt{E\Gamma_0/(1-\nu^2)}$. The only *independent* material-based length parameter in the present study is R_S. It is important to appreciate that R_S is *not* the plastic zone size of a mode II crack with specific microscopic work of fracture Γ_0— that plastic zone size would generally be much larger, i.e., given by (3) with the specific macroscopic work of mode II fracture Γ_{II} replacing Γ_0. In earlier work on mode I cracking, Tvergaard and Hutchinson [6] introduced the corresponding length for a tensile crack $R_0 = [1/(3\pi(1-\nu^2)]E\Gamma_0/\sigma_Y^2$, which is $R_S/9$. With Γ_{CROP} as the specific work expended by the cropping plunger (per area of plate cut) for long straight cuts, two dimensionless forms for the specific cropping work in terms of the parameters identified above will be considered

$$\frac{\Gamma_{\mathrm{CROP}}}{\tau_Y h} = g_1\left(\frac{h}{R_S}, \frac{\hat{\tau}}{\tau_Y}, N, \frac{d}{h}, \frac{\tau_Y}{E}\right) \tag{4}$$

$$\frac{\Gamma_{\mathrm{CROP}}}{\Gamma_0} = g_2\left(\frac{h}{R_S}, \frac{\hat{\tau}}{\tau_Y}, N, \frac{d}{h}, \frac{\tau_Y}{E}\right) \tag{5}$$

where the dependence on ν has not been noted explicitly, and

$$g_1 = \frac{\Gamma_0}{\tau_Y h} g_2 = \pi(1-\nu^2)\frac{\tau_Y}{E}\frac{R_S}{h} g_2 \tag{6}$$

Both normalizations will be used to reveal important aspects of the parametric dependencies. For example, it will be seen that the dependence on τ_Y appears mainly through the first two dimensionless parameters in g_2 in (5) and not through the fifth parameter τ_Y/E, while g_1 in (4) has a strong dependence on τ_Y/E in its list of parameters.

The preferred dimensionless relation relating the cropping force per length F with units $\mathrm{Nm}^{-1} = \mathrm{Jm}^{-2}$, and the displacement of the cropping tool through which it works Δ is

$$\frac{F}{\tau_Y h} = g_3\left(\frac{\Delta}{h}, \frac{h}{R_S}, \frac{\hat{\tau}}{\tau_Y}, N, \frac{d}{h}, \frac{\tau_Y}{E}\right) \tag{7}$$

By (4), one notes that $g_1 = \int_0^1 g_3 d(\Delta/h)$.

3 Prescription of the Computational Model

3.1 The Cohesive Zone. As noted above, a cohesive zone model is used to characterize the strength and fracture interface of the plane along which cutting occurs. Because the cutting process is not strictly shearing, a mixed mode traction-separation law is employed in the form introduced in [7] for studying mixed mode interface crack growth. While the tangential displacement δ_t across the failure plane is expected to dominate the cutting behavior, the model also accounts for a normal separation δ_n. Denote the critical value of δ_t at which the traction vanishes under strictly shearing as δ_t^c and similarly denote the critical strictly normal separation by δ_n^c. Under mixed mode conditions, the displacement measure $\lambda = \left[\left(\delta_n/\delta_n^c\right)^2 + \left(\delta_t/\delta_t^c\right)^2\right]^{1/2}$ is employed such that the tractions drop to zero at $\lambda = 1$. The tractions are derived from a potential function given by

$$\Phi(\delta_n, \delta_t) = \delta_t^c \int_0^\lambda \tau(\lambda')d\lambda' \tag{8}$$

where $\tau(\lambda)$ characterizes the traction–separation relation in shear. Use of the potential results in a work of cohesive failure that is the same for all mixed mode separations, which is given by (8) with $\lambda = 1$, i.e., $\Gamma_0 = \delta_t^c \int_0^1 \tau(\lambda')d\lambda'$. The normal and tangential components of the traction acting on the cohesive failure plane are given by

$$T_n = \frac{\partial \Phi}{\partial \delta_n} = \frac{\tau(\lambda)}{\lambda}\frac{\delta_n}{\delta_n^c}\frac{\delta_t^c}{\delta_n^c}, \quad T_t = \frac{\partial \Phi}{\partial \delta_t} = \frac{\tau(\lambda)}{\lambda}\frac{\delta_t}{\delta_t^c} \tag{9}$$

In this paper the following piecewise linear traction–separation law is used (see Fig. 3(*a*)):

$$\tau(\lambda) = \frac{\lambda}{\lambda_1}\hat{\tau} \quad \text{for } 0 \le \lambda < \lambda_1 \tag{10}$$

$$\tau(\lambda) = \hat{\tau} \quad \text{for } \lambda_1 \le \lambda < \lambda_2 \tag{11}$$

$$\tau(\lambda) = \frac{1-\lambda}{1-\lambda_2}\hat{\tau} \quad \text{for } \lambda_2 \le \lambda < 1 \tag{12}$$

Here $\hat{\tau}$ denotes the maximum shear traction sustained by the failure plane under a mode II shear, i.e., $\delta_n = 0$. The peak normal traction under mode I separation is $\hat{\sigma} = \left(\delta_t^c/\delta_n^c\right)\hat{\tau}$. The specific work of separation per unit area of interface is

$$\Gamma_0 = \frac{1}{2}\hat{\tau}\delta_t^c(1 - \lambda_1 + \lambda_2) \tag{13}$$

In all the simulations carried out in this paper, the values $\lambda_1 = 0.15$ and $\lambda_2 = 0.5$ have been used such that $\Gamma_0 = 0.675\hat{\tau}\delta_t^c$. Studies of mode I and mixed mode crack growth in elastic–plastic solids indicated that the detailed shape of the traction–separation law as determined by λ_1 and λ_2 are less important than Γ_0 and $\hat{\tau}$ [6,7], and this is expected to be true for cropping as well.

3.2 The Elastic–Plastic Constitutive Behavior and the Finite Element Model. The cropped material is elastic–plastic, with the elastic modulus and Poisson's ratio E and ν, uniaxial yield stress σ_Y, and strain hardening exponent N. This material is described by a finite strain generalization of J_2-flow theory [17], with the uniaxial true stress–natural strain curve represented by a piecewise power law

$$\varepsilon = \begin{cases} \dfrac{\sigma}{E} & \sigma \le \sigma_Y \\ \dfrac{\sigma_Y}{E}\left(\dfrac{\sigma}{\sigma_Y}\right)^{1/N} & \sigma > \sigma_Y \end{cases} \tag{14}$$

A Lagrangian convected coordinate formulation of the field equations is used for the analyses, with a material point identified by the coordinates x_i in the reference configuration, accounting for finite strains. The contravariant components of the Cauchy stress tensor σ^{ij} and the Kirchhoff stress tensor τ^{ij} are related by $\tau^{ij} = \sqrt{G/g}\,\sigma^{ij}$. The metric tensors in the current and reference configurations are denoted by G_{ij} and g_{ij}, with determinants G and g, and the incremental stress–strain relationship is of the form $\dot{\tau}^{ij} = L^{ijkl}\dot{\eta}_{kl}$, where L^{ijkl} are the instantaneous moduli.

The Lagrangian strain tensor is given by

$$\eta_{ij} = \frac{1}{2}\left(u_{i,j} + u_{j,i} + u^k_{,i}u_{k,j}\right) \tag{15}$$

where u^i are the displacement components on the reference base vectors and $()_{,j}$ denotes covariant differentiation in the reference frame. Numerical solutions are obtained by a linear incremental solution procedure, based on the principle of virtual work

$$\int_V \tau^{ij}\delta\eta_{ij}dV + \int_{S_I}\{T_n\delta(\delta_n) + T_t\delta(\delta_t)\}dS = \int_S T^i\delta u_i dA \tag{16}$$

Here V and S are the volume and surface of the body in the reference configuration, respectively, S_I is the bonded surface cohesive region, and T^i are contravariant components of the nominal surface tractions. An incremental version of the PVW (16) is used for the numerical solution. The displacement fields are approximated in terms of planar eight-noded isoparametric elements. The volume integral in Eq. (16) is carried out by using 2×2 integration points within each element.

The region analyzed numerically is specified by $-a \le x_2 \le a$ and $0 \le x_1 \le h$ in terms of the reference coordinates x_i (see Fig. 3(*b*)). The plunger is pressed against the surface $-a \le x_2 \le -d$ at $x_1 = 0$, with the plunger displacement Δ in the x_1 direction. The plate is supported on the back surface $d \le x_2 \le a$ at $x_1 = h$ with zero displacement in the x_1 direction.

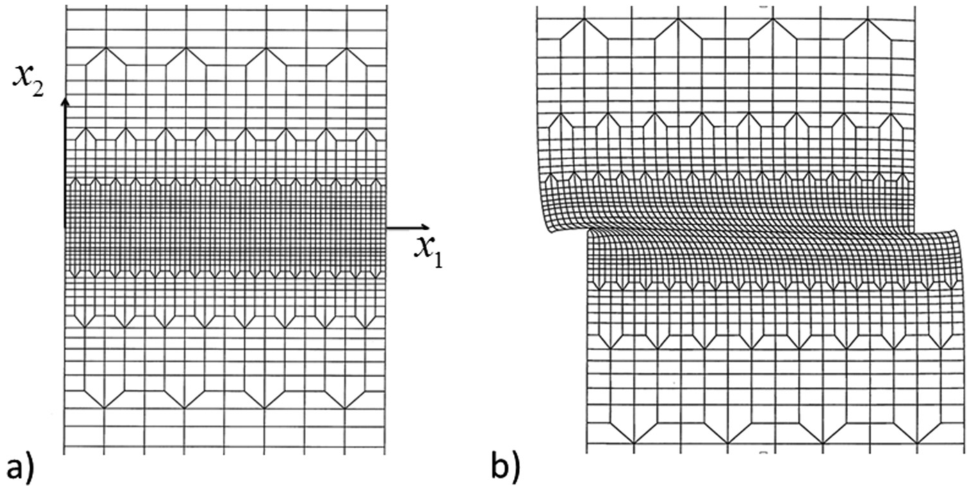

Fig. 4 (*a*) The mesh in the undeformed state. The cohesive plane lies along the x_1 axis. (*b*) The deformed mesh for the reference case (case 1) at $\Delta/h = 0.136$.

The cohesive plane, on which shear localization and failure is modeled, coincides with the x_1 axis. In all but two of the simulations, the gap d between the plunger and the cohesive plane is taken to be zero. Full sticking is assumed at both the plunger and the support so that zero displacement in the x_2 direction is prescribed at these surfaces. Even though this is a plane strain analysis, the displacements in the x_2 direction are prescribed to be zero at the lower edge $x_2 = -a$, for $0 \le x_1 \le h$, thus modeling an effect similar to that at the centerline for circular geometries such as that in Fig. 1. The surface at $x_2 = a$ is traction-free. The initial geometry is here taken to be specified by $h/a = 0.8$. Figure 4(*a*) shows the initial mesh in the vicinity of the cohesive interface, with 64×4 uniform quadrilaterals on each side of the interface. The length of one square element inside this uniformly meshed region is denoted D_0. To adequately resolve the fracture process, the length of the active process region (i.e., the region where $\lambda_1 < \lambda < 1$) should not be smaller than three or four times this element length D_0.

Figure 4(*b*) shows the deformed mesh at $\Delta/h = 0.136$ for the reference case (case 1). This is just before the point where the full cross section at the interface has attained $\lambda \ge \lambda_1$, i.e., the equivalent of localization in the cohesive plane. A numerical difficulty encountered in this case with $d = 0$ is that nodal points on the cohesive interface very near the corner of the plunger approach final separation $(\lambda \ge 1)$ slowly. A few interface nodal points on the plunger side moved past the plunger corner resulting in significant mesh distortion. This difficulty was resolved by prescribing that no nodal points on the plunger side of the interface can move past the current location of the corner of the plunger. The problem does not arise in analyses where the value of the normalized peak stress $\hat{\tau}/\tau_Y$ is sufficiently small, but becomes pronounced when the value of the normalized peak stress is in the upper range considered in this paper.

4 Trends in Cropping Force and Work

In this section the results from a selection of simulations will be presented to expose the roles of the parameters identified in Sec. 2 on the cropping force–displacement behavior and the macroscopic work of cropping. A total of 21 simulations have been carried out. The dimensionless parameters for each simulation are listed in Table 1 and identified by a case number. The four primary parameters are h/R_S, $\hat{\tau}/E$, N, and τ_Y/E. The thickness of the plate enters only through h/R_S. An alternative dimensionless parameter to h/R_S is

$$\frac{h\tau_Y}{\Gamma_0} = \frac{E}{\pi(1-\nu^2)\tau_Y}\frac{h}{R_S} \tag{17}$$

which is also listed in Table 1.

Case 1 in Table 1 will be used at the reference case throughout this paper. The dimensionless parameters for case 1 are believed to be representative of a plate of a tough, intermediate strength steel of several millimeters thickness, such as the DH 36 plate discussed in the Introduction. Neither $\hat{\tau}/\tau_Y$ nor h/R_S are known for this material, or any other comparable material, and thus the choices for these parameters must be regarded as educated guesses. In addition to the parameters listed in Table 1, the other parameters which must be specified in the simulation code are taken as

$$\nu = 0.3, \quad \lambda_1 = 0.15, \quad \lambda_2 = 0.5, \quad \delta_n^c/\delta_t^c = 1$$

The first three are used in all the simulations. Simulations with values of δ_n^c/δ_t^c other than 1 have been carried out and will be reported later, but δ_n^c (and $\hat{\sigma} = (\delta_t^c/\delta_n^c)\hat{\tau}$) have very little effect on

Table 1 Simulation cases[a]

Case	$\frac{h}{R_s}$	$\frac{\hat{\tau}}{\tau_Y}$	N	$\frac{\tau_Y}{E}$	$\frac{d}{h}$	$\frac{\sigma_{PS}}{\sigma_Y}$	$\frac{h\tau_Y}{\Gamma_0}$*	$\frac{\Gamma_{CROP}}{\Gamma_0}$	$\frac{\Gamma_{CROP}}{\tau_Y h}$
1 (R)	0.0427	3.12	0.185	0.000785	0	1	19.0	6.11	0.321
2	0.0427	3.12	0.185	0.000393	0	1	38.0	6.59	0.173
3	0.0427	3.12	0.185	0.001570	0	1	9.51	5.07	0.533
4	0.0427	3.12	0.125	0.000785	0	1	19.0	11.90	0.626
5	0.0427	3.12	0.156	0.000785	0	1	19.0	9.46	0.498
6	0.0427	3.12	0.227	0.000785	0	1	19.0	3.69	0.194
7	0.0427	3.12	0.33	0.000785	0	1	19.0	1.85	0.0973
8	0.0480	2.77	0.185	0.000785	0	1	21.4	4.53	0.212
9	0.0384	3.46	0.185	0.000785	0	1	17.1	7.99	0.467
10	0.0427	2.77	0.185	0.000785	0	1	19.0	4.27	0.224
11	0.0427	3.46	0.185	0.000785	0	1	19.0	8.55	0.450
12	0.0854	3.12	0.185	0.000785	0	1	38.0	9.02	0.237
13	0.0284	3.12	0.185	0.000785	0	1	12.7	4.91	0.387
14	0.0214	3.12	0.185	0.000785	0	1	9.51	4.08	0.429
15	0.0256	3.46	0.185	0.000785	0	1	11.4	5.99	0.526
16	0.0192	3.46	0.185	0.000785	0	1	8.56	4.94	0.578
17	0.0427	3.12	0.185	0.000785	0	1.2	19.0	6.08	0.320
18	0.0427	3.12	0.185	0.000785	0	2.0	19.0	5.55	0.292
19	0.0427	3.12	0.185	0.000785	0.031	1	19.0	11.96	0.630
20	0.0427	3.12	0.185	0.000785	0.047	1	19.0	14.20	0.747
21	0.0427	3.12	0.185	0.000785	0	1	19.0	6.01	0.316

[a] In all calculations: $\nu = 0.3$, $\lambda_1 = 0.15$, $\lambda_2 = 0.50$, and $\delta_n^c/\delta_t^c = 1$ (except for 21, $\delta_n^c/\delta_t^c = 1/2$). Case 1 is the reference case and denoted by a subscript R in the text and figures.
* $h\tau_Y/\Gamma_0$, given by (17), is not an independent parameter.

the predictions due to the dominance of shearing in the cropping process.

4.1 The Role of h/R_S—Specifically, the Role of the Specific Microscopic Work of Fracture Γ_0 and/or the Plate Thickness h. In this set of simulations, N and τ_Y/E are fixed and h/R_S is varied for two choices of $\hat{\tau}/\tau_Y$. By (17), for each choice of $\hat{\tau}/\tau_Y$, varying h/R_S is equivalent to varying $h\tau_Y/\Gamma_0$. In other words, if one considers all the other *dimensional* parameters as being fixed, this set of simulations is equivalent to either varying only Γ_0 with h fixed or varying h with Γ_0 fixed. For this set of simulations, varying only Γ_0 is accomplished by varying only δ_t^c [cf. (13)]. Figure 5 displays the dimensionless force–displacement curves. The influence of the parameter h/R_S (or, equivalently, $h\tau_Y/\Gamma_0$) on the force–displacement behavior is significant, especially so considering that dimensionless results for any model based only on plastic shearing alone cannot contain a dependence on h, at least assuming that there is no gap $d=0$. This assertion follows from the dimensional argument that the only parameter containing a length dimension available to combine with h to form a dimensionless parameter is Γ_0, e.g., h/R_S or $h\tau_Y/\Gamma_0$.

Values of the two dimensionless measures of the specific cropping work are given in Table 1. While it is essential to make use of dimensionless parameter combinations for problems such as cropping, which have a large number of independent parameters, relations among dimensionless variables often mask connections between dimensional quantities. This is particularly true for the specific work of cropping. Thus, to clearly display the effect of the specific microscopic work of fracture Γ_0 on the specific work of cropping Γ_{CROP}, normalized variables are used in Fig. 6 with $\Gamma_{CROP}/(\Gamma_{CROP})_R$ plotted as a function of $\Gamma_0/(\Gamma_0)_R$ for plates with the same thickness h. Here, and subsequently, the subscript R denotes a value from Table 1 for the reference case 1. These same curves provide the relation between $\Gamma_{CROP}/(\Gamma_{CROP})_R$ and $(h)_R/h$ for plates having the same Γ_0. Clearly the specific microscopic work of fracture has significant influence on the specific macroscopic cropping work, even though Γ_0 is a small fraction of Γ_{CROP} (cf. Table 1). The quantitative predictions in Fig. 6 back up the earlier modeling of Atkins [1–4], who seems to be the first to view cropping as a shear fracture problem and not just a plastic shear-off process.

The curves in Fig. 6 also reveal the effect of plate thickness on the specific cropping work for the reference material. Doubling

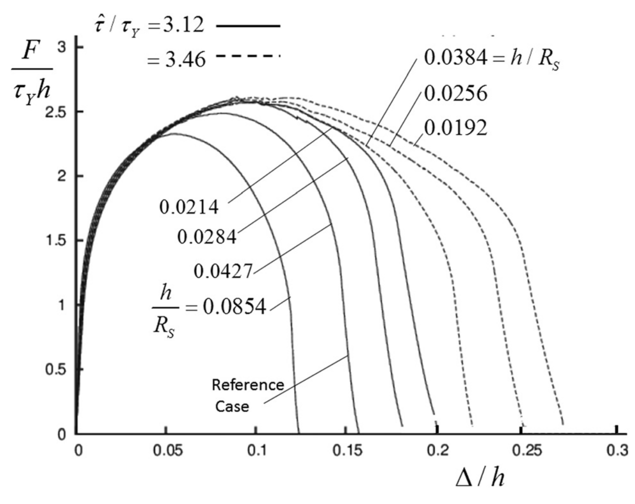

Fig. 5 The role of $h/R_S=\pi(1-\nu^2)h\tau_Y^2/(E\Gamma_0)$ on the normalized force–displacement relation for cropping for two values of $\hat{\tau}/\tau_Y$ and with $N=0.185$ and $\tau_Y/E=0.000785$. With all the other dimensional parameters fixed, each set of curves (for a given $\hat{\tau}/\tau_Y$) can be interpreted as either the effect of varying Γ_0 (with h fixed) or varying h (with Γ_0 fixed). Cases 1, 11, 12, 13, 14, 15, and 16.

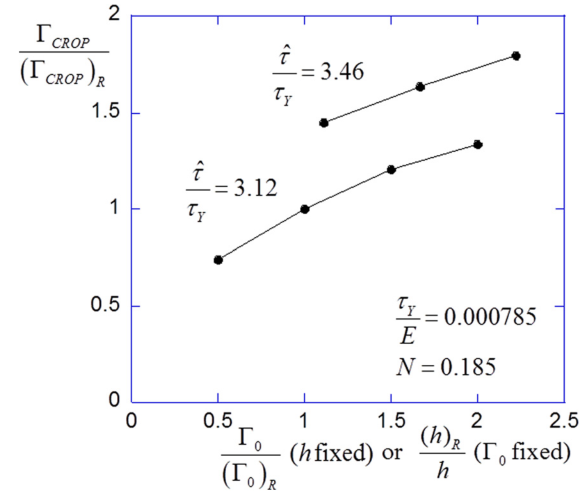

Fig. 6 The dependence of the specific cropping work Γ_{CROP} on the microscopic specific work of fracture Γ_0 for plates of the same thickness. Equivalently, the dependence of the specific cropping work Γ_{CROP} on inverse thickness $1/h$ for plates with fixed material properties. The normalizing quantities denoted by the subscript R refer to reference case 1. The points plotted are cases 1, 11, 12, 13, 14, 15, and 16.

the thickness decreases Γ_{CROP} by about 30%, and vice versa. Recall that both Γ_{CROP} and Γ_0 are defined as energy per separated area, with units Jm^{-2}. Thus, the simulations predict that the total work required to crop a plate of the considered material increases by only a factor of about 1.4 when the thickness of the plate is doubled—much less than the factor of 2 expected if Γ_{CROP} were independent of thickness. Conversely, cropping a plate of this material with half the thickness only reduces the total cropping work by a factor of about 0.7 rather than 0.5. This dependency on plate thickness is not at all obvious. However, it follows directly from dimensional arguments that there must be a dependence of Γ_{CROP} on h if there is a dependence on Γ_0—as noted above, the only length parameter in the problem that can be used to form a dimensionless parameter involving Γ_0 is h.

The several stages of the cropping process are indicated in Fig. 7 for the reference case. The entire cropping region undergoes extensive plastic yielding through the thickness of the plate prior to the onset of any crack growth. The fully plastic nature of the cropping process, emphasized in the Introduction, is evident in Fig. 7 where large nonlinear displacements due to plasticity occur prior to any cracking. At the maximum load, the shear cracks emerging from the corners of the platens have grown to a length of approximately $h/20$. With further imposition of the cropping displacement, each zone of shear decohesion extends towards the center of the plane until, at $\Delta/h \cong 0.14$, they merge at the center. Prior to this point in the process, significant plastic deformation takes place outside the cohesive zone. However, for $\Delta/h > 0.14$, the deformation is mainly confined to the cohesive zone, the cracks grow toward each other, and the cropping force drops dramatically until the cracks connect at the center at $\Delta/h \cong 0.16$.

There are some differences between the sequence of events occurring in Fig. 7 and those laid out in the early work of Johnson and Slater [14]. These authors argued that at the time their paper was written there was no evidence for shear cracking prior to the maximum punch force, and they suggest that the maximum is a result of shear localization. In their view, cracking first occurs after the maximum load is attained. Specific details such as these will depend on the tendency for a given material to undergo shear localization prior to shear damage. To some extent, the sequence of events can be explored within the context of the present model by varying the cohesive zone parameters. For example, decreasing the shear strength $\hat{\tau}$ while fixing, or increasing, the specific work

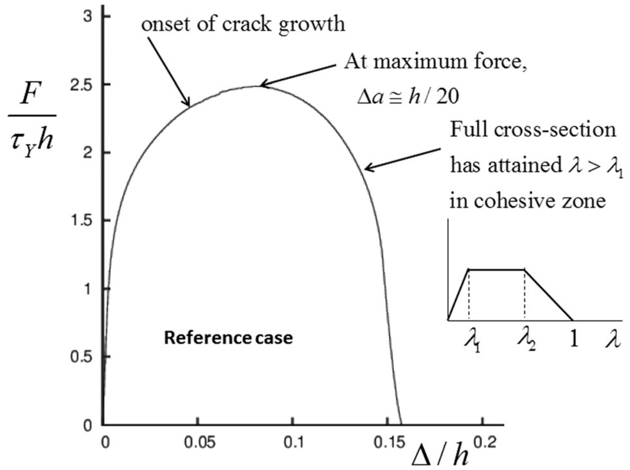

Fig. 7 Three stages of the cropping process illustrated for the reference case. (i) Onset of cracking when λ first attains 1 in the cohesive zones at the corners of the cropping tool. (ii) At maximum force the cracks at each corner of the tool on opposite surfaces have extended a distance approximately 1/20th the plate thickness. (iii) The point at which the traction plateau is attained in the cohesive zone throughout the central cross section of the plate, i.e., $\lambda \geq \lambda_1$. As Δ increases beyond this point, localized shear-off is confined to the cohesive zone and the cracks spread toward the center until they meet at $\Delta/h \cong 0.16$. Case 1.

of fracture Γ_0 promotes early localization relative to shear cracking. In addition, Johnson and Slater [4] discuss the role friction is expected to play once a shear crack has developed. Friction is not taken into account in the present model and; thus, the cropping force vanishes when the cracks connect.

4.2 The Role of the Normalized Shear Strength $\hat{\tau}/\tau_Y$.

In this set of simulations h/R_S, N, and τ_Y/E are fixed at the reference values and $\hat{\tau}/\tau_Y$ is varied. To generate the force–displacement curves presented in Fig. 8 and the associated values of the cropping work in Table 1, both $\hat{\tau}$ and δ_t^c are varied such that $\Gamma_0 = 0.675\hat{\tau}\delta_t^c$ and h are unchanged. The microscopic shear strength $\hat{\tau}$ obviously has significant effect on both the maximum cropping force and the cropping work. The dimensionless cropping work from Table 1 for these three cases are $\Gamma_{\mathrm{CROP}}/\Gamma_0 = 4.27, 6.11, 8.55$ for $\hat{\tau}/\tau_Y = 2.77, 3.12, 3.46$, respectively. This strong dependency is similar to the role that the cohesive tensile strength plays in mode I crack growth resistance in small scale yielding [6].

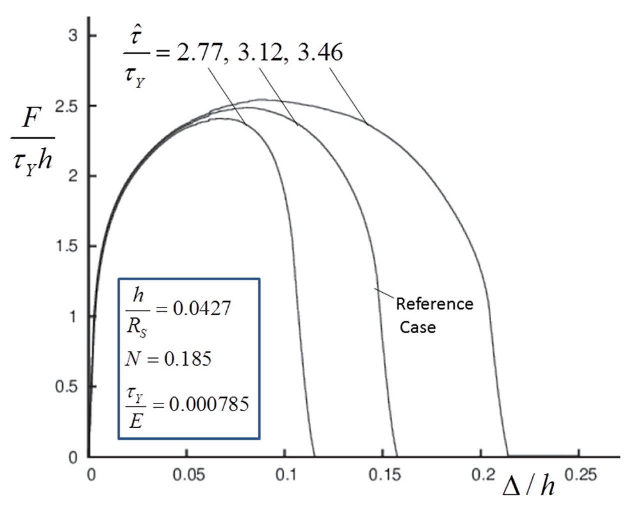

Fig. 8 The role of the normalized shear strength in the cohesive zone $\hat{\tau}/\tau_Y$ on the normalized force–displacement curve with the other dimensionless parameters held fixed. Cases 1, 10, and 11.

The cropping process is dominated by shear both in the cohesive zone and in the surrounding field of plasticity as the strong dependence on $\hat{\tau}$ reflects. All but one of the simulations listed in Table 1 take $\delta_n^c/\delta_t^c = 1$, which by the cohesive law (9) implies that under a purely normal separation the peak stress would be $\hat{\sigma} = (\delta_t^c/\delta_n^c)\hat{\tau} = \hat{\tau}$. For most materials this would be an unusually low peak for normal separation. To see the effect of the parameter δ_n^c/δ_t^c on the cropping process, a simulation (case 21) was carried out with dimensionless parameters identical to those of the reference case except with $\delta_n^c/\delta_t^c = 1/2$ corresponding to $\hat{\sigma} = 2\hat{\tau}$. Both the normalized force–displacement curve and the normalized specific cropping work (see Table 1) were essentially unchanged from the reference case 1. For the present model, the mixed mode cohesive characteristics as determined by δ_n^c/δ_t^c have almost no influence on cropping, at least with no gap $(d/h = 0)$, consistent with the notion that cropping is dominated by shearing.

4.3 The Role of Strain Hardening N.

The simulated force–displacement curves in Fig. 9 show the effect of varying N with the other dimensionless parameters held fixed. Increased strain hardening elevates the cropping force, but makes it easier to attain the tractions required to cause cohesive shear. The result is that higher strain hardening decreases the normalized displacement Δ/h at which the cropping force become zero. With fixed τ_Y, the cropping work is also a strong function of N, varying from $\Gamma_{\mathrm{CROP}}/\tau_Y h = 0.0973$ for $N = 0.33$ to $\Gamma_{\mathrm{CROP}}/\tau_Y h = 0.626$ for $N = 0.125$ (Table 1). Of course, for a family of alloys, processing treatments that increase N are usually accompanied by a decrease in τ_Y, and thus, when that is the case, a change in the parameter τ_Y/E must also be taken into account.

4.4 The Role of τ_Y/E.

In this subsection, the effect of changes in τ_Y/E with h/R_S, $\hat{\tau}/\tau_Y$, and N held fixed are examined. To carry out these calculations, E was changed, but to ensure that h/R_S did not change, Γ_0 was also changed such that the product $E\Gamma_0$ was fixed. The normalized force displacement curves are shown in Fig. 10, where the influence of τ_Y/E is seen to be significant. The role of τ_Y (or E) is not easy to decipher because it is present in three (two) of the dimensionless parameter combinations. While the dimensionless specific work of cropping $\Gamma_{\mathrm{CROP}}/\tau_Y h$ is strongly affected by variations in τ_Y/E, the second measure in Table 1 $\Gamma_{\mathrm{CROP}}/\Gamma_0$ is only weakly dependent on τ_Y/E. A fourfold change in τ_Y/E (with h/R_S, $\hat{\tau}/\tau_Y$, and N fixed) produces only about a 25% change in $\Gamma_{\mathrm{CROP}}/\Gamma_0$. The important conclusion to be drawn is that the cropping work as measured by $\Gamma_{\mathrm{CROP}}/\Gamma_0$ depends primarily on h/R_S, $\hat{\tau}/\tau_Y$, and N.

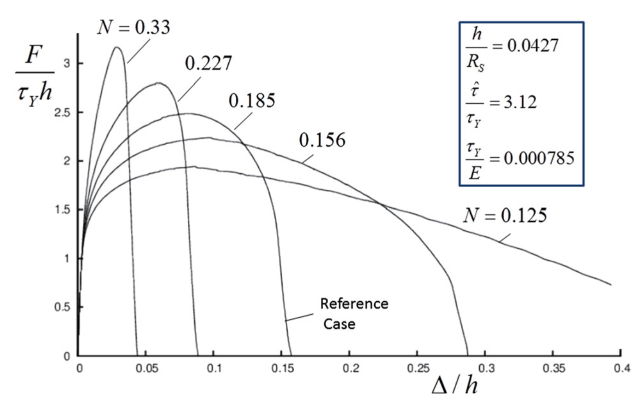

Fig. 9 The role of the strain hardening exponent on the normalized force–displacement curves with the other dimensionless parameters held fixed. Cases 1, 4, 5, 6, and 7.

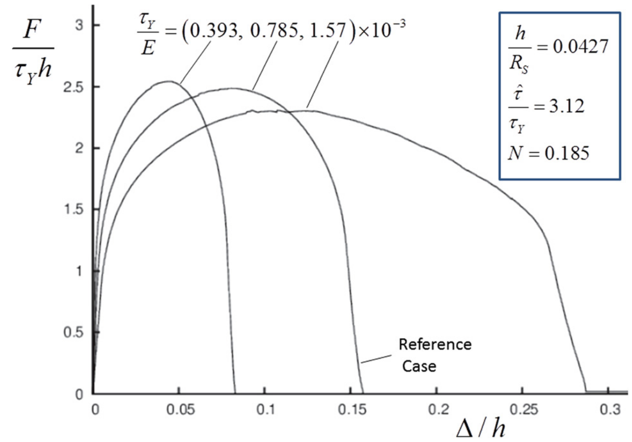

Fig. 10 The role of τ_Y/E on the normalized force–displacement curves with the other dimensionless parameters held fixed. As discussed in the text, the specific cropping work with the normalization Γ_{CROP}/Γ_0 is only weakly dependent on τ_Y/E with the other dimensionless parameters held fixed. Cases: 1, 2, and 3.

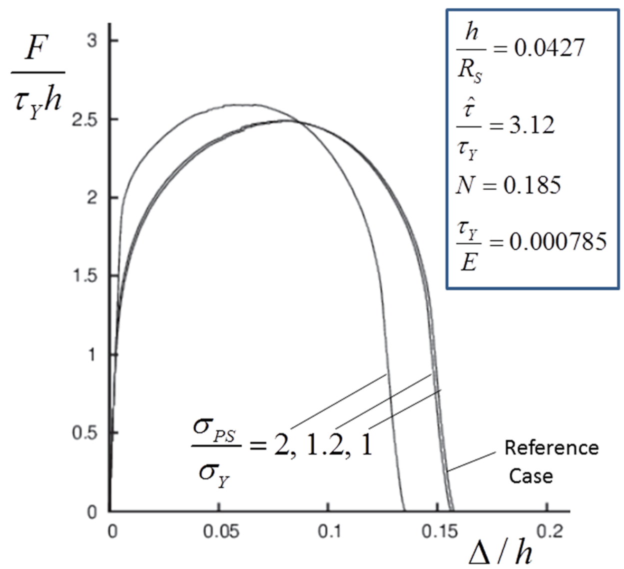

Fig. 11 A tensile prestress σ_{PS} is applied to the plate to produce uniform plastic stretch and then released prior to cropping. The other dimensionless parameters for the prestress cases (cases 17 and 18) are the same as for case 1, the reference case.

4.5 The Role of Prestress σ_{PS}/σ_Y. To illustrate one possible application of the model, the effect of uniform prestraining [1] is considered. Assume the plate is strained in uniaxial tension beyond yield to a stress σ_{PS} then released to the unstressed state prior to cropping. This prestressing is accounted for in the cropping simulations by simply expanding the starting radius of Mises yield surface from its initial value associated with σ_Y to the value associated with σ_{PS}. Case 17, with $\sigma_{PS}/\sigma_Y = 1.2$, and case 18, with $\sigma_{PS}/\sigma_Y = 2$, given in Table 1, have their other parameters identical to those of the reference, case 1. (In Table 1, for all the other cases, $\sigma_{PS}/\sigma_Y = 1$ has been used to indicate there has been no plasticity due to prestress.) The cropping force–displacement curves in Fig. 11 reveal that a small prestress $\sigma_{PS}/\sigma_Y = 1.2$ has essentially no effect on cropping. However, the larger value $\sigma_{PS}/\sigma_Y = 2$ has a noticeable effect on the cropping curve and reduces the specific work of cropping by about 10%.

4.6 The Role of the Gap d/h. A few computations have been carried out to study the effect of a cropping gap. Specifically, for case 19, the initial gap between the edge of the plunger and the cohesive plane was taken to be two element sizes, $d = 2D_0$, and the same gap is assumed at the edge of the supporting tool. Thus, the cohesive plane coincides with the center of the gap. If the mesh in Fig. 4(*a*) is used, strong mesh distortion at the edge of the plunger leads to early breakdown of the computation. Therefore, a specially refined mesh is used around the point where intense straining is induced at the edge of the plunger, as shown in Fig. 12(*a*). This enables the computation to proceed, but the material in the gap rotates significantly, even to the extent that it overlaps the material under the plunger. Consequently, an extra condition is introduced stipulating that the material in the gap cannot penetrate the plunger, as illustrated by the deformed mesh in Fig. 12(*b*). This contact condition is taken to be frictionless sliding.

The normalized force–displacement curves for two gaps sizes $d/h = 0.031$ and 0.047 are presented in Fig. 13 along with that for the reference case (case 1) which has no gap but otherwise identical parameters. A gap has a significant influence resulting in larger plastic deformation accompanying the cropping process. For the smaller of the two gap sizes, $d/h = 0.031$, the cropping work is approximately twice that of the reference case (cf. Table 1).

As indicated by the above discussion, the large plastic strain and extensive rotation accompanying the shear decohesion process is challenging to simulate, especially when a gap is present. More extensive studies accounting for the gap are clearly required. Handbook rules exist recommending maximum gap to thickness ratios for cropping; modeling these rules is part of the challenge ahead. It should also be mentioned that the effect of changing the relative tensile strength in the cohesive zone

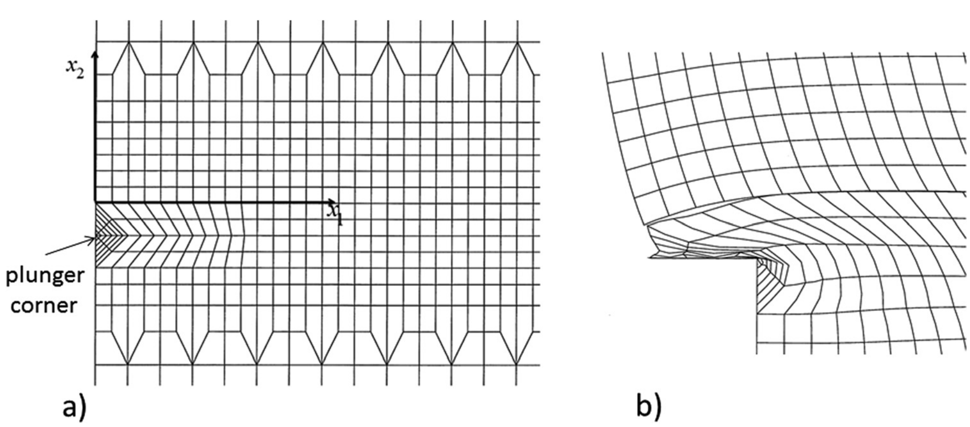

Fig. 12 (*a*) Undeformed mesh for simulation with a gap $d = 2D_0$. (*b*) Deformed mesh with gap in the vicinity of the plunger corner for case 19 at $\Delta/h = 0.108$.

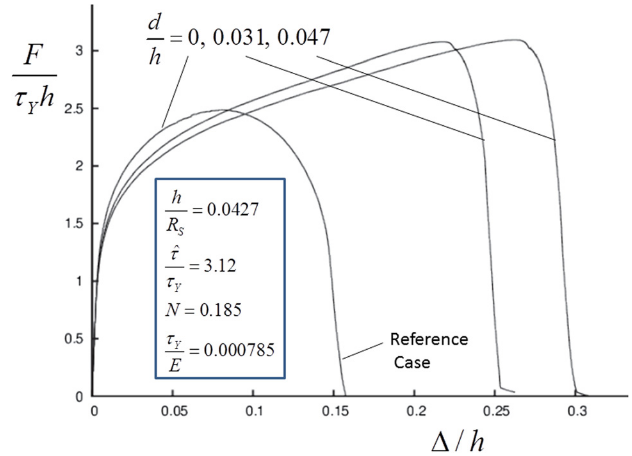

Fig. 13 The role of a gap between the tool corners and the cohesive plane d/h on the normalized force–displacement curves with the other dimensionless parameters held fixed and equal to those of the reference case. Cases: 1, 19, and 20.

$\hat{\sigma} = (\delta_t^c/\delta_n^c)\hat{\tau}$ has not been studied in the presence of a gap when it is more likely to be important [5].

5 Concluding Remarks

Cropping falls within the larger field concerned with the mechanics and physics of cutting [18]. The present paper has introduced a model which links macroscopic aspects of cropping, such as the cropping force–displacement behavior and the work of cropping, to properties at the microscopic scale such as the fundamental fracture energy of the material and its shear strength. Predictions based on the model have been presented to reveal trends in this relationship. In the examples presented in the body of the paper, the specific macroscopic work of cropping ranges from 2 to 15 times the specific microscopic work of fracture. Nevertheless, even when the microscopic work of fracture comprises only a small fraction of the total work, it has been shown to play a critical role in establishing the macroscopic behavior. The present cropping study parallels earlier efforts to predict the macroscopic mode I fracture toughness of ductile metal alloys in terms of more fundamental microscopic material properties [6]. In so doing, the present study advances the case made by Atkins [1–4] that cropping should be viewed as a fracture problem. In the terminology of nonlinear fracture mechanics, cropping is a large scale yielding fracture problem. Cropping presents its own special challenges owing to the large plastic strains that inevitably accompany the process and the fact that shear localization and shear fracture are less well understood in terms of fundamental material mechanisms than the tensile fracture of ductile metals under high stress triaxiality. The challenges are both computational and physical.

As mentioned in connection with the introduction of the reference case, the choices of the peak shear strength and work of fracture characterizing the cohesive zone have not been directly calibrated with experiments. For example, it is possible that the microscopic parameters of the steel DH36 lie outside the range covered by the simulations in this paper. The fact that the plunger displacement at failure $\Delta/h \cong 0.5$ for the DH36 test in Fig. 1(*b*) is larger than any of the values found in the present simulations suggests this might be the case. The main purpose of the present paper has been to expose trends in the roles of the parameters controlling cropping. Future efforts will be undertaken to make direct comparisons with cropping experiments. Finally, it must be reemphasized that important factors could be added to the present model which have not be taken into account, such as tool deformation, friction, and material temperature and rate dependence.

References

[1] Atkins, A. G., 1980, "On Cropping and Related Processes," Int. J. Mech. Sci., **22**(4), pp. 215–231.
[2] Atkins, A. G., 1981, "Surfaces Produced by Guillotining," Philos. Mag. A, **43**(3), pp. 627–641.
[3] Atkins, A. G., 1990, "On the Mechanics of Guillotining Ductile Metals," J. Mater. Proc. Tech., **24**, pp. 245–247.
[4] Atkins, T., 2012, "Perforation of Metal Plates Due to Through-Thickness Shearing and Cracking. Optimum Toughness/Strength Ratios, Deformation Transitions and Scaling," Int. J. Impact Eng., **48**, pp. 4–14.
[5] Zhou, Q., and Wierzbicki, T., 1996, "A Tension Zone Model of Blanking and Tearing of Ductile Metal Plates," Int. J. Mech. Sci., **38**(3), pp. 303–324.
[6] Tvergaard, V., and Hutchinson, J. W., 1992, "The Relation Between Crack Growth Resistance and Fracture Process Parameters in Elastic–Plastic Solids," J. Mech. Phys. Solids, **40**(6), pp. 1377–1397.
[7] Tvergaard, V., and Hutchinson, J. W., 1993, "The Influence of Plasticity on Mixed Mode Interface Toughness," J. Mech. Phys. Solids, **41**(6), pp. 1119–1135.
[8] Borvik, T., Langseth, M., Hoppenstad, O. S., and Malo, K. A., 1999, "Ballistic Penetration of Steel Plates," Int. J. Impact Eng., **22**(9-10), pp. 855–886.
[9] Borvik, T., Hoppenstad, O. S., Berstad, T., and Langseth, M., 2002, "Perforation of 12 mm Steel Plates by 20 mm Diameter Projectiles With Flat, Hemispherical and Conical Noses: Part II: Numerical Simulations," Int. J. Impact Eng., **27**(1), pp. 37–64.
[10] Nahshon, K., Pontin, M. G., Evans, A. G., Hutchinson, J. W., and Zok, F. W., 2007, "Dynamic Shear Rupture of Steel Plates," J. Mech. Mater. Struct., **2**(10), pp, 2049–2065.
[11] Xue, Z., Pontin, M. A., Zok, F. W., and Hutchinson, J. W., 2010, "Calibration Procedures for a Computational Model of Ductile Fracture," Eng. Fracture Mech., **77**(3), pp. 492–509.
[12] Gurson, A. L., 1977, "Continuum Theory of Ductile Rupture by Void Nucleation and Growth—I. Yield Criteria and Flow Rules for Porous Ductile Media," ASME J. Eng. Mater. Technol., **99**(1), pp. 2–15.
[13] Nahshon, K., and Hutchinson, J., 2008, "Modification of the Gurson Model for Shear Failure," Eur. J. Mech./A Solids, **27**(1), pp. 1–17.
[14] Johnson, W., and Slater, R. A. C., 1967, "A Survey of the Slow and Fast Blanking of Metals at Ambient and High Temperatures," International Conference on Manufacturing Technology (CIRP-ASTME), Ann Arbor, MI, September, pp. 825–851.
[15] Tvergaard, V., 2009, "Behaviour of Voids in a Shear Field," Int. J. Fracture, **158**(1), pp. 41–49.
[16] Tvergaard, V., and Nielsen, K. L., 2010, "Relations Between a Micro-Mechanical Model and a Damage Model for Ductile Failure in Shear," J. Mech. Phys. Solids, **58**(9), pp. 1243–1252.
[17] Hutchinson, J. W., 1973, "Finite Strain Analysis of Elastic–Plastic Solids and Structures," *Numerical Solution of Nonlinear Structural Problems*, R. F. Hartung, ed., ASME, New York, pp. 17–29.
[18] Atkins, T. 2009, *The Science and Engineering of Cutting*, Butterworth-Heinemann, London.